Hindawi
Laser and Particle Beams
Volume 2023, Article ID 3125787, 12 pages
https://doi.org/10.1155/2023/3125787

Research Article

A Methodology for the Discrimination of Alpha Particles from Other Ions in Laser-Driven Proton-Boron Reactions Using CR-39 Detectors Coupled in a Thomson Parabola Spectrometer

Vasiliki Kantarelou,[1] **Andriy Velyhan**,[1] **Przemysław Tchórz**,[2] **Marcin Rosiński**,[2] **Giada Petringa**,[1,3] **Giuseppe Antonio Pablo Cirrone**,[1,3] **Valeriia Istokskaia**,[1,4] **Josef Krása**,[5] **Miroslav Krůs**,[6] **Antonino Picciotto**,[7] **Daniele Margarone**,[1,3,8] **and Lorenzo Giuffrida**[1,3]

[1]*ELI Beamlines Facility, The Extreme Light Infrastructure ERIC, Dolni Brezany, Czech Republic*
[2]*Institute of Plasma Physics & Laser Microfusion (IPPLM), Warsaw, Poland*
[3]*Southern National Laboratory (LNS), Istituto Nazionale Fisica Nucleare, Catania, Italy*
[4]*Czech Technical University in Prague, Faculty of Nuclear Sciences and Physical Engineering, Prague, Czech Republic*
[5]*FZU-Institute of Physics, Czech Academy of Sciences, Prague, Czech Republic*
[6]*Institute of Plasma Physics, Czech Academy of Sciences, Prague, Czech Republic*
[7]*Micro-Nano Facility, Fondazione Bruno Kessler, Trento 38123, Italy*
[8]*Centre for Light-Matter Interactions, School of Mathematics and Physics, Queen's University Belfast, Belfast, UK*

Correspondence should be addressed to Vasiliki Kantarelou; vasiliki.kantarelou@eli-beams.eu

Received 1 December 2022; Revised 1 February 2023; Accepted 14 February 2023; Published 27 February 2023

Academic Editor: Sergey Pikuz

Solid-state nuclear track detectors (CR-39 type) are frequently used for the detection of ions accelerated by laser-plasma interaction because they are sensitive to each single particle. To the present day, CR-39 detectors are the main diagnostics in experiments focused on laser-driven proton-boron ($p^{11}B$) fusion reactions to detect alpha particles, which are the main products of such a nuclear reaction, and to reconstruct their energy distribution. However, the acceleration of multispecies ions in the laser-generated plasma makes this spectroscopic method complex and often does not allow to unambiguously discriminate the alpha particles generated from $p^{11}B$ fusion events from the laser-driven ions. In this experimental work, performed at the PALS laser facility (600 J, 300 ps, laser intensity 10^{16} W/cm^2), CR-39 detectors were used as main detectors for the angular distribution of the produced alpha particles during a $p^{11}B$ fusion dedicated experimental campaign. Additionally, a CR-39 detector was set inside a Thomson Parabola (TP) spectrometer with the aim to calibrate the CR-39 response for low energetic laser-driven ions originating from the plasma in the given experimental conditions. The detected ion energies were ranging from hundreds of keV to a few MeV, and the ion track diameters were measured for etching times up to 9 hours. The goal of the test was the evaluation of the detectors' ability to discriminate the alpha particles from the aforementioned ions. Within this study, the calibration curves for protons and silicon low energy ions are accomplished, the overlapping of the proton tracks and alpha particles is verified, and a methodology to avoid this problem is realized.

1. Introduction

Nowadays, the interest of the scientific community involved in the study of the laser-driven nuclear reactions is growing because of the possible multidisciplinary applications. Although the fusion reaction between tritium and deuterium is still considered the most interesting among other fusion reactions considered for

power generation [1], the one between hydrogen and ^{11}B nucleus, called proton-boron nuclear fusion reaction ($p^{11}B$) [2], represents a complementary and potentially alternative solution in future advanced schemes. In fact the possibility to generate three alpha particles per single reaction, with a negligible generation of neutrons, makes this type of reaction of interest in many fields of research (for a futuristic nuclear plant [3], in space applications [4], in cancer treatment [5, 6], in radioisotope production [7], or in material science).

As reported in the literature, this nuclear reaction has a main resonance occurring at 670 keV of proton energy in the center of mass frame, with the cross section of 1.2 barn and a secondary resonance peak at 170 keV energy in the center of mass (0.1 barn). The generated alpha particles have a broad energy spectrum with the main peak at around 4 MeV and a cut-off energy at 7 MeV [8, 9].

Since 2005, the $p^{11}B$ reaction has been triggered by the use of ultra-high intense laser systems [10–14], and despite the impressive progresses in the alpha particle rate enhancement [15], an extensive systematic investigation of laser-based $p^{11}B$ fusion and deep understanding of the underpinning physics is still missing [16].

As of today, in the experimental study of the $p^{11}B$ fusion reaction, one of the critical experimental bottlenecks is the definition of a trustable detector allowing to discriminate the alpha particles from the other charged particles produced from the plasma source. This issue is related with the clear understanding and interpretation of the experimental results [17].

In this direction, solid-state nuclear track detectors, CR-39 type, have proved to be a reliable diagnostic tool for the characterization of the energy distribution of alpha particles generated by the laser-driven proton-boron fusion. In fact, they are extremely sensitive to a single incident particle and are not affected by the intense electromagnetic noise produced in the laser-target interaction [18].

One of the issues related with the use of such as passive diagnostic is that a calibration is needed to correlate the diameter of the tracks created by the particles caught in the detector surface during the irradiation to the corresponding incident energy and to the ion species. The calibration curves can be produced by the irradiation of the CR-39 detectors with monochromatic ions that can be generated by accelerators or radioactive sources. Although the use of CR-39 detectors appears to be straightforward, the major difficulty of their application relies on the fact that the same size of a track can correspond to two different energies of the same particle or to two different ions with different energies.

Within this study, we propose an alternative calibration technique for the CR-39 detectors and a simple method to discriminate the alpha particles generated in a $p^{11}B$ reaction from concurrent protons and other ions at given experimental conditions.

2. Materials and Methods

The current experiment was realized during a $p^{11}B$ nuclear reaction experiment at the Prague Asterix Laser System (PALS) in Czech Republic [19]. The PALS laser is an iodine laser working at the fundamental wavelength of 1315 nm, ~800 J maximum laser energy on the target, and sub-ns pulse duration (0.3 ns FWHM). The laser was focused on the sample with an incidence angle of 30° to the target normal reaching an intensity of $1 \cdot 10^{16}$ W/cm^2.

A Thomson Parabola spectrometer (TP) was placed at 0° along the target normal and 1.58 m away from the target. The laser-driven ions were collimated by a 200 μm diameter pinhole before entering the TP as sketched in Figure 1.

The produced ions are deflected when they pass through electric and magnetic fields mutual parallel and perpendicular to the beam axis. The electric field causes a deflection in one direction (x axis) that it is proportional to the E_i/Z ratio, where E_i is the energy of the ion and Z is the ion charge. The magnetic field deflects the ions proportionally to the m_i/Z ratio in a perpendicular direction (y axis), where m_i is the mass of the ion. Therefore, the ions with higher charge and lower kinetic energy will deflect more and ions with the same mass over charge ratio will group on the same parabola [20, 21].

The parabolas are usually recorded by an imaging plate. Within the current experiment, the electric and magnetic fields applied were 500 kV/m and 168 mT, respectively, and the parabolas were partially recorded by CR-39 nuclear track detectors that were placed on top of the imaging plate. The energies of the detected ions calculated by the analytical formulas of the parabolas were crosschecked by simulation using the SIMION software [22].

Within this study, we present results originating from the CR-39 used as focal plane detector in the TP detecting ions from the interaction of the laser with a SiHB target.

The operation of the CR-39 detectors is based on the damage of the molecular chains of polymers by the passage of charged particles that leave tracks on their way. The irradiated detectors are placed in a sodium hydroxide (NaOH) or a potassium hydroxide (KOH) solution at a certain temperature (ranging from 60 to 90°C) to be etched. Afterwards the etched detectors are analyzed with a high-resolution optical microscope to measure the diameter of the recorded tracks and their number.

The track diameter is related to the energy of the impinging particle, thus allowing reconstructing the energy distribution of the ion beam, as well as its flux [23]. Many studies describe the dependence of the track diameter with the energy of the different ions, mostly referred to protons, alpha particles, and carbon ions [23–35]. However, the calibration of CR-39 for other species such as boron and silicon ions is almost missing in the current bibliography.

The dependence of the track diameter on the ion energy can be described as follows: in the low energy region, the diameter of the track grows rapidly with the energy until a threshold is reached, after which the diameter decreases as the energy of the ion increases. This behavior follows the stopping power shape of the ion inside the materials [25, 36] and at the same etching conditions and etching time: (a) ions with higher stopping power values create bigger tracks and (b) ions of the same species but with different energy cause bigger tracks when their energy is closer to the stopping power maximum.

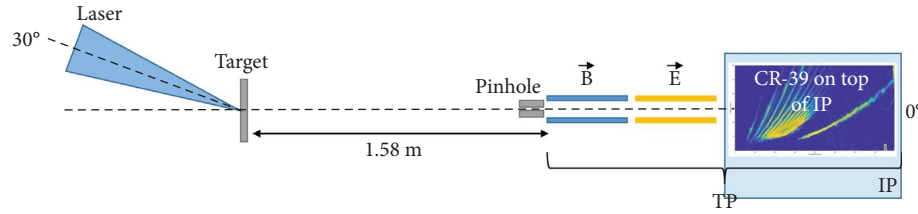

FIGURE 1: Scheme of the experimental setup, CR-39 detector was placed on top of the TP imaging plate, covering part of its surface.

The detectors energy calibration can be performed by irradiating them with monochromatic ion beams at conventional accelerator facilities or by using radioactive sources. The laser-driven ion beams are not monoenergetic and therefore cannot be used as an ion source to precisely calibrate the CR-39 detectors unless a control spectral dispersion is used. In [26, 30, 37], CR-39 detectors have been calibrated for protons, carbons, deuterons, and nitrogen ions in laser facilities, and in the current experiment, we used a similar configuration.

The SiHB targets presented in this paper were realized in a complementary metal-oxide-semiconductor (CMOS) fabrication pilot line, the class-10 clean room for device microfabrication at the micro and nanofacility of the Fondazione Bruno Kessler in Trento (Italy) [38–40]. So, the developed process is compatible with standard CMOS processing, which allows a direct transfer of the technology. Targets were made starting from 6-inch standard CZ (Czochralski) <100> silicon wafers with a thickness of 300 μm. By silicon microfabrication technological processes, a series of free-standing membranes of about 2 microns of thickness has been realized. These last were subsequently doped by boron ion implantation ($D = 10^{17}$ cm^{-2}; $E = 50$ keV) and enriched by hydrogen atmosphere for 3 hours at a temperature of 420°C by using a thermal annealing furnace. Even if the natural isotope abundance of the boron is 80% for ^{11}B and 20% of ^{10}B, the ion implanter utilized in that experiment (like all systems worthy of the name) they possess an analyzing magnet selecting the right mass on charge ratio (m/q), in our case for the p^{11}B we need ^{11}B. The possible presence of the boron 10 inside the target is certainly in a negligible concentration.

After the laser-target interaction, protons, silicon, boron, carbon ions (originating from surface contaminations), and alpha particles, emerging from the p^{11}B nuclear reactions, were generated and detected by the CR-39 detectors located inside the TP.

After the irradiation, the CR-39 were etched for 9 hours in a NaOH 6.25 M solution at 70°C. The tracks were recorded after every hour of etching with an optical microscope [41]. An example of an irradiated detector with tracks of different ions, after 8 h of etching is presented in Figure 2. The signal less deflected in the vertical direction originates from the protons that are the most energetic, followed by the different charge states of heavier ions (silicon, boron, and carbon).

3. Results and Discussion

Three different shots and, consequently, three CR-39s have been analyzed, as summarized in Table 1. On the first and second CR-39, with dimensions 2×2 cm^2, protons were detected with energies between 0.22 – 0.41 MeV and 0.31–0.92 MeV, respectively. On the third detector (Figure 2) with bigger dimensions (2×3 cm^2), the detection of protons (0.9–1.75 MeV) and silicon ions (0.56–12.9 MeV) was possible.

The detection of B and C ions was not possible due to their parabolas are very close to Si ones as it is determined from their Z/m ratio. In Table 1, we shortened the Z/m ratios of each produced ion from the smallest ratio to the biggest one. From this, it is evident that the following pairs of B and Si ions have parabolas that are very close: (B^{+1}, Si^{+3}), (B^{+2}, Si^{+6}), (B^{+3}, Si^{+8}), (B^{+4}, Si^{+11}), or completely overlapped (B^{+5}, C^{+6}, He^{+2}, Si^{+12}). Additionally, the boron element being a dopant inside the SiHB target has lower concentration than Si resulting to fewer production of B ions with respect to the Si ones. For these reasons, the detection of B ions was not possible. The C ions, being present as a contaminant from the surface are produced in smaller amounts (with respect to the Si ones) only C^+ was possible to detect and only at 9 h of etching because the tracks were not well defined from the early etching times. Regarding the He ions, He^{+1} parabola overlaps with C^{+3} and Si^{+7} ones making their detection impossible.

Unfortunately, the detection of alpha particles was not realized as well due to the production of Si^{+14} and B^{+5} ions that overlap the parabola of alpha particles having the same Z/m ratio. Additionally, it should also be noted that the number of the produced alpha particles is negligible with respect to the other ion signals, and therefore, their tracks can easily be "hidden" inside the common parabola. This is supported from a previous p^{11}B experiment at PALS [15] where the number of the produced alpha particles from a hydrated Si target was estimated at 10^9 p/sr/shot. This flux would result to an entrance of 13 alpha particles/shot inside the TP.

A summary of the detected ions and their energy at the CR-39 is presented in Table 2, together with all information about the target and laser parameters used during this test. Carbon ions (C^{+1}) were recorded only at 9 h of etching because the tracks were not well defined from the early etching times.

The proton and silicon parabolas were fully documented by taking subsequent pictures moving the microscope vertically on the sample from the upper area (away from the pinhole) to the bottom (closer to the pinhole). Each picture corresponds to different vertical positions without overlapping or gaps between the images. Then, the pictures were grouped in groups of ten (squares in Figure 3(a)) and were analyzed using the ImageJ [42] software.

Figure 3(a) presents the proton signal from the TP of the first shot here under study. The squares in Figure 3(a) represent the grouped analyzed areas. The area of each

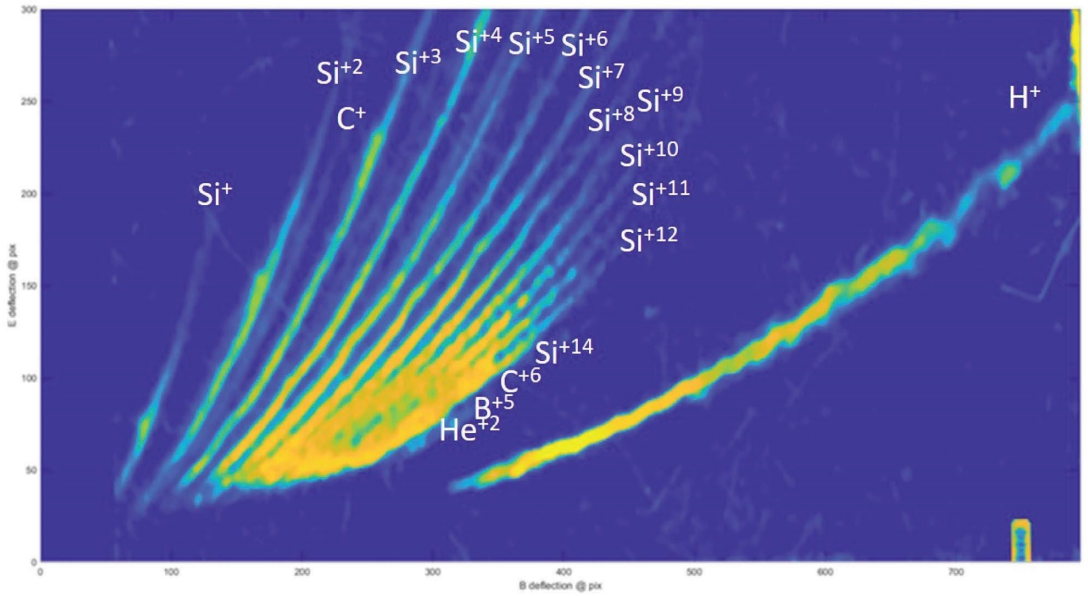

Figure 2: Image of ion parabolas recorded on the CR-39 detector after the irradiation of SiHB target as obtained after 8 h of etching.

Table 1: The charge over mass ratio of each produced ion.

Ion species	Z/m
Si^{+}	0.035714
Si^{+2}	0.071429
C^{+}	0.083333
B^{+}	0.1
Si^{+3}	0.107143
Si^{+4}	0.142857
C^{+2}	0.166667
Si^{+5}	0.178571
B^{+2}	0.2
Si^{+6}	0.214286
Si^{+7}	0.25
He^{+1}	0.25
C^{+3}	0.25
Si^{+8}	0.285714
B^{+3}	0.3
Si^{+9}	0.321429
C^{+4}	0.333333
Si^{+10}	0.357143
Si^{+11}	0.392857
B^{+4}	0.4
C^{+5}	0.416667
Si^{+12}	0.428571
Si^{+13}	0.464286
Si^{+14}	0.5
He^{+2}	0.5
C^{+6}	0.5
B^{+5}	0.5
H^{+}	1

group on the parabola corresponds to a mean energy of the tracks. The analysis of each group provided a Gaussian-like distribution of the diameters of the detected tracks (Figure 3(b)). The maximum of each Gaussian distribution corresponds to the mean diameter of the analyzed tracks. With this method, we correlated the energy of the analyzed tracks with respect to the diameters of the tracks and accordingly we produce the calibration curves. In Figure 3(b), the colors of the Gaussians correspond to the same-colored areas (squares) from Figure 3(a). In this example, the diameters are becoming wider in the direction from the top of the CR-39 (away from the pinhole) to the bottom (i.e., from the black area to the purple one). This means that the tracks from the particles with higher energy are bigger; this is correct in this case because the detected energies are less than 0.5 MeV, which is lower than the expected maximum (in diameters) in the calibration curve. Therefore, the track diameters increase with the energy increment. Figure 3(c) presents the calibration curves for protons as it was produced from all three different shots and for different etching times (2–9 hours).

For the sake of completeness, a comparison between the calibration curve obtained from the TP in this work, the calibration from a previous study, done using a conventional accelerator at INFN in Catania, and one from reference [25] is presented in Figure 4. These calibrations were performed using the same etching conditions and the same etching time, 8 h. The graphic shows that the TP results (here referred as "current work" and presented in black circle) are in excellent agreement with the literature results from [25], (red circles), while exhibit at least 30% difference (if we take into account the errors in diameters and energy) with the previous results from INFN, (blue circles). However, we should also point out that calibration curves that are carried out in different laboratories even if they are produced from the same experimental campaigns might vary due to the use of a different setup (microscopes, etching baths, software for the analysis of the tracks, and mainly because of a different operator).

From the parabolas, it was possible to extract useful information for the calibration of CR-39 for the Si^{+} in the energy range between 0.5 and 1.9 MeV. Figure 5 presents the

Table 2: Detected ions and their energy at each CR-39 detector.

Shot number	Laser energy (J)	Target	CR-39	Dimensions (cm^2)	Detected ions: energy range (MeV)
55872	589	SiHB	1	2×2	p^+: 0.22–0.41
55873	588		2	2×2	p^+: 0.31–0.91 p^+: 0.90–1.75
55882	661		3	2×3	Si: 0.59–12.9 C: 0.25–1.88

calibration curves of Si^+ from 2 h up to 9 h of etching. The results show that, in this case, the diameter of the tracks increases with the increment of the energy. This behavior was expected since the energy of the ions is small, away from the maximum in stopping power.

In Figure 6, the diameters of the tracks of Si +1, +2, +3, +4, and +12 are also included for 9 h of etching. The analysis of the rest of the silicon ions was not possible since their parabolas were either too close one to the other causing saturation or they contained more than one ion track species, which were not discernible. However, the analysis of these parabolas would not provide more data since they correspond to energies that are already reported (the minimum and the maximum energies are determined by the energies of Si +1 and +12, respectively) and therefore would not improve the graph in Figure 6. A fitting procedure of the experimental data was introduced to determine the energy dependence of the diameter of the tracks. The diameter (D in μm) exhibits an exponential grow dependence with the energy (E in MeV) of the Si ions within the specific energy range (0.5–14 MeV). The fitting relation is as follows:

$$D = A \bullet e^{(E/b)} + C, \quad (1)$$

where $A = -21.1341 \pm 0.51717$, $b = -3.39641 \pm 0.27833$, and $C = 27.07478 \pm 0.59134$

A comparison between the calibration curves of protons, silicon, and carbon ions at 9 h of etching is presented in Figure 7. The diameters of the different ions have similar sizes at the low energy region (below 2 MeV) suggesting that the discrimination of the particles is not always possible. The inset in Figure 7 shows a zoom in the energies below 2 MeV where we can see that the protons with energies between 0.2 and 0.7 MeV correspond to diameters 9.6–14.8 μm, which also correspond to silicon and carbon ions with energies between 0.7–1.4 and 0.46–1.34 MeV, respectively. Furthermore, protons with energies between 1.24 and 1.75 MeV form tracks with diameters between 7.3 and 4.6 μm, which correspond to silicon and carbon ions with energies less than 0.7 and 0.3 MeV, respectively. However, this situation is valid only for the specific etching time, and therefore, the results must be evaluated case by case.

Figure 8 shows that the tracks of Si^+ are distinguishable from the ones of the proton tracks for the first three hours of etching (Figure 8(a)). From 4 to 6 hours the Si tracks that correspond to energies below 1 MeV have similar sizes with the protons tracks (Figure 8(b)). Then, up to 8 hours, the Si tracks that correspond to energies below 1.2 MeV are not distinguishable from proton tracks (Figure 8(c)) and finally at 9 hours Si tracks up to 1.8 MeV have similar sizes with the proton tracks (Figure 8(d)).

This can be explained by the difference of the tracks etching growth. Figure 9 shows the evolution of the diameters for protons and Si^{+1} of 0.5 MeV through etching time. Although proton tracks exhibit a linear growth with time, Si ion tracks stop growing after 3 h of etching. The diameters of Si ions from 4 h to 9 h of etching have a mean value of 5.8 ± 0.9 μm. Although the respective diameter at 4 h of etching has a lower value, it also includes a big error and fits inside this interval. This behavior of the etching growth can be attributed to the fact that the Si tracks are superficial (1 MeV Si ions is stopped at 2 μm inside the CR-39), and consequently, after 3 h of etching the exposed surface of the detector has reached the damaged zone resulting in slow growth. This is analytically described in [36] where the depth dependence of track etch rate and of the restricted energy loss (REL) are presented. The track etch rate and the REL reach a maximum at the same depth of the detector and then the etch rate decreases rapidly. Consequently, the evolution of a track almost stops when the etched surface of the detector nearly matches the bottom of the track. This means that although Si ions form tracks that have bigger diameters from the proton ones; after some hours of etching (in our laboratory 4 h), the difference in their growth result to similar sized tracks. For this reason, we believe that long etching hours should be avoided.

Finally, we evaluate the potential of the CR-39 detectors to discriminate the alpha particles from protons and silicon ions during a $p^{11}B$ experiment. We coupled the alpha particle track calibration curve with the experimental ones (from TP) of protons and silicon ions at 2 h of etching, as shown in Figure 10. The calibration of CR-39 for alpha particles was realized at LNL-INFN accelerators (AN2000 and CN) in Legnaro, Italy [43], but the detectors were analyzed in our laboratory. This graph shows that the tracks of alpha particles overlap mostly with the ones from silicon ions in the range of diameters between 3–4.8 μm (red area in the graph). Therefore, the alpha particles with energies between 0.5 and 3.15 MeV form same sized tracks with the Si ions with energies between 0.5 and 1.25 MeV. Additionally, the alpha tracks overlap with the proton ones in the range 1.7–2.6 μm; black area in the graph that correspond to protons with energies 0.39–0.87 MeV and alpha particles with energies 4–4.8 MeV. However, the lower limitation in diameters (and consequently the higher detected energies) in our calibration curve is not absolute. The trend of the calibration curves shows that alpha particles with energy higher than 4.8 MeV should create tracks with diameters less than 1.7 μm. This means that the alpha tracks with energies above 4 MeV have the same size with all the protons in our

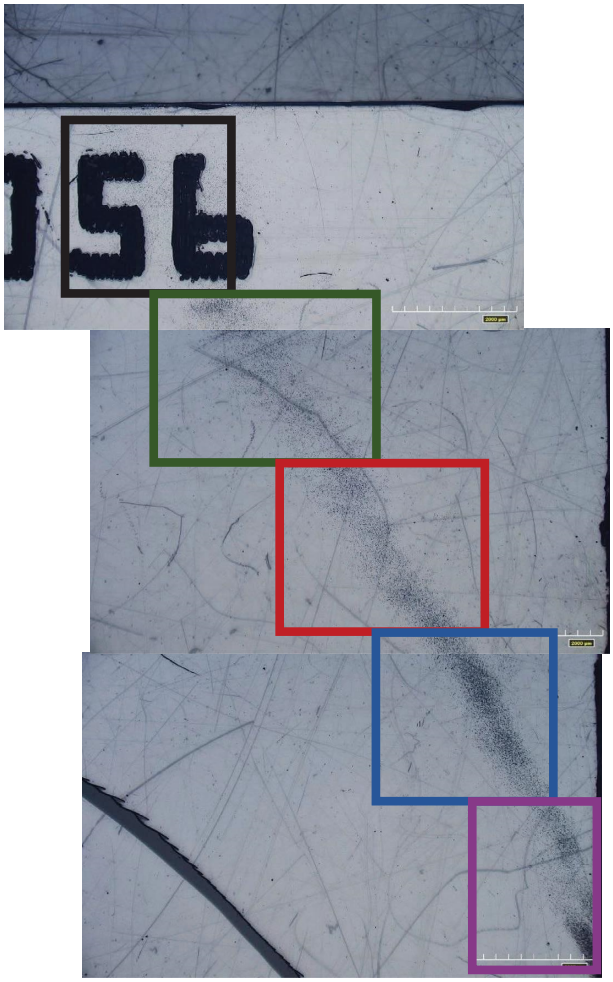

(a)

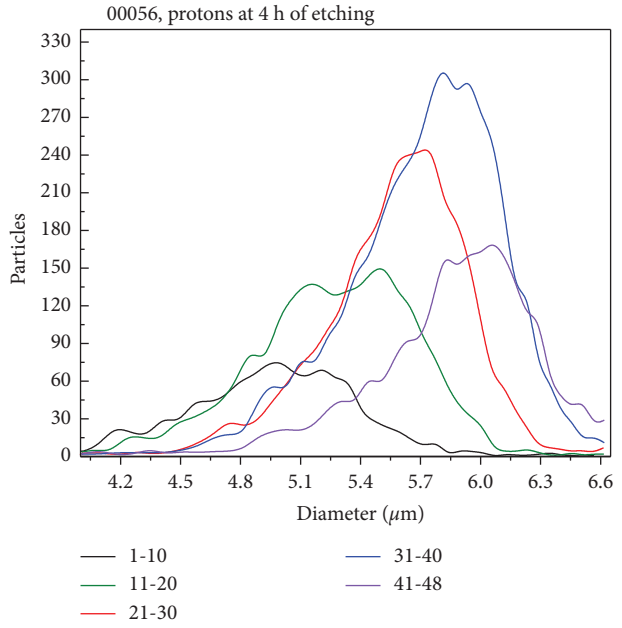

(b)

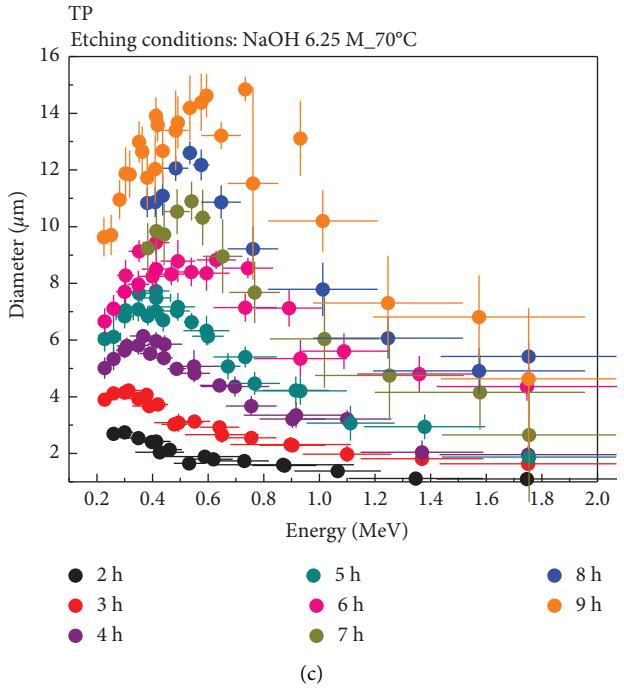

(c)

FIGURE 3: (a) Stitched images showing the full proton parabola from the TP as registered on the CR-39. The colored squares represent different regions analyzed. (b) The analysis of each group (of 10 pictures) resulted a Gaussian-like distribution of the diameters of the detected tracks. The colors of the Gaussians correspond to the same colored rectangular form (a). (c) Dependence of the diameter of protons at a function of the proton energy for different etching times.

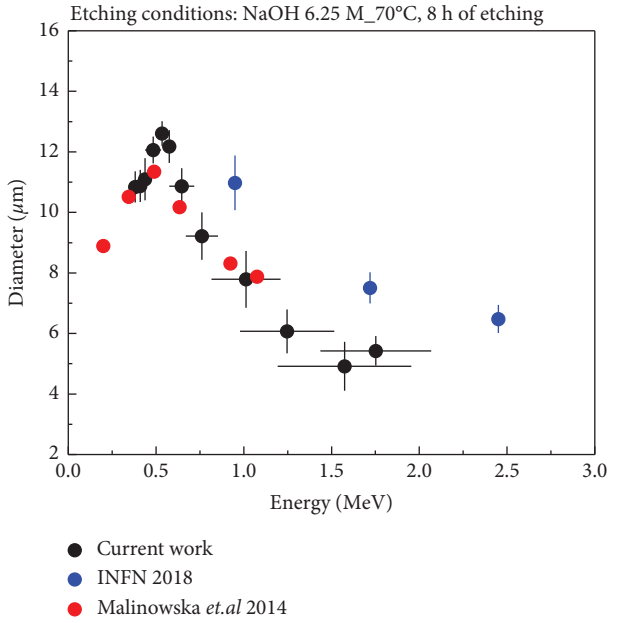

Figure 4: Comparison of our experimental results (current work) with results from INFN and from [20]. The diameters calculated from TP (black circles) are in excellent agreement with the ones from bibliography (red circles). However, there is a big difference (more than 30%) from the INFN results (blue circles).

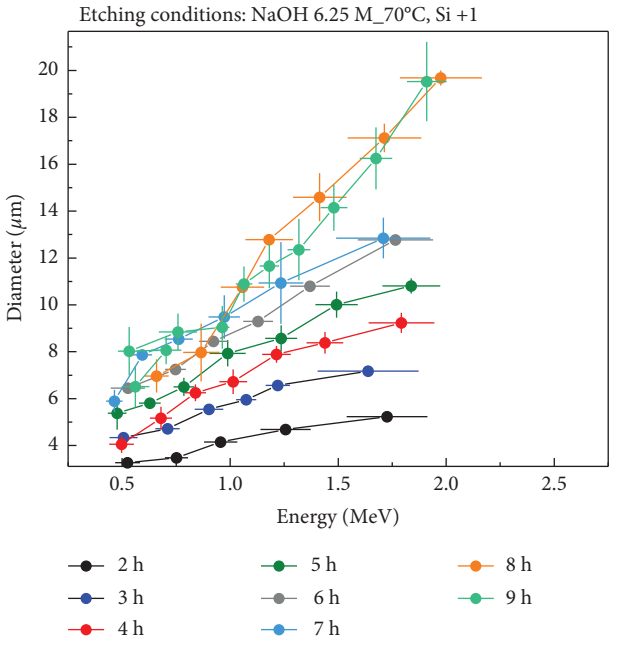

Figure 5: Calibration curves of Si^+ ions from 2 h up to 9 h of etching time.

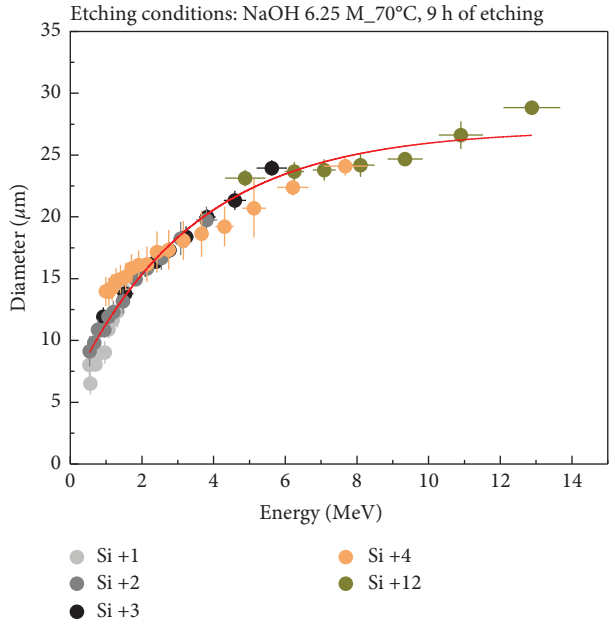

Figure 6: Calibration curve for the Si +1, +2, +3, +4, and + 12 ions, a fitting procedure (red line in the graph) shows the energy dependence of the diameters.

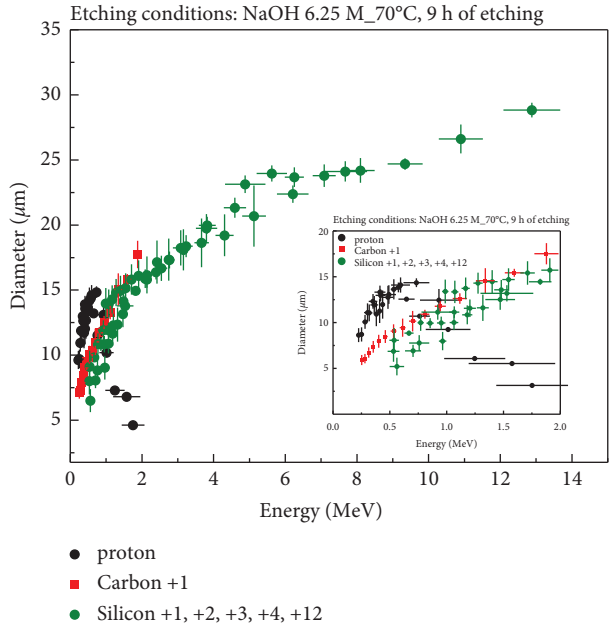

Figure 7: Diameters versus energy for protons, Si and C +1 ions for 9 h of etching. The inset presents a zoom in the energy region below 2 MeV. The results suggest the discrimination of protons from Si and C ions is not possible for energies below 2 MeV.

calibration curve (above 0.39 MeV). Apparently, the alpha tracks overlap fully with Si and proton tracks at 2 h of etching. Nevertheless, in the case of silicon ions, their discrimination from the alpha particles can be achieved by the use of proper filtering that can be placed in front of the CR-39 that would prevent their passage on the detectors' surface. For example, in our case, an Al filter with thickness 6 μm would exclude all silicon ions with energies below 13 MeV and alpha particles and protons with energies below 1.7 and 0.6 MeV, respectively.

A different approach should be adopted for the discrimination of alpha particles from protons since a thicker filter would exclude firstly the detection of alpha particles.

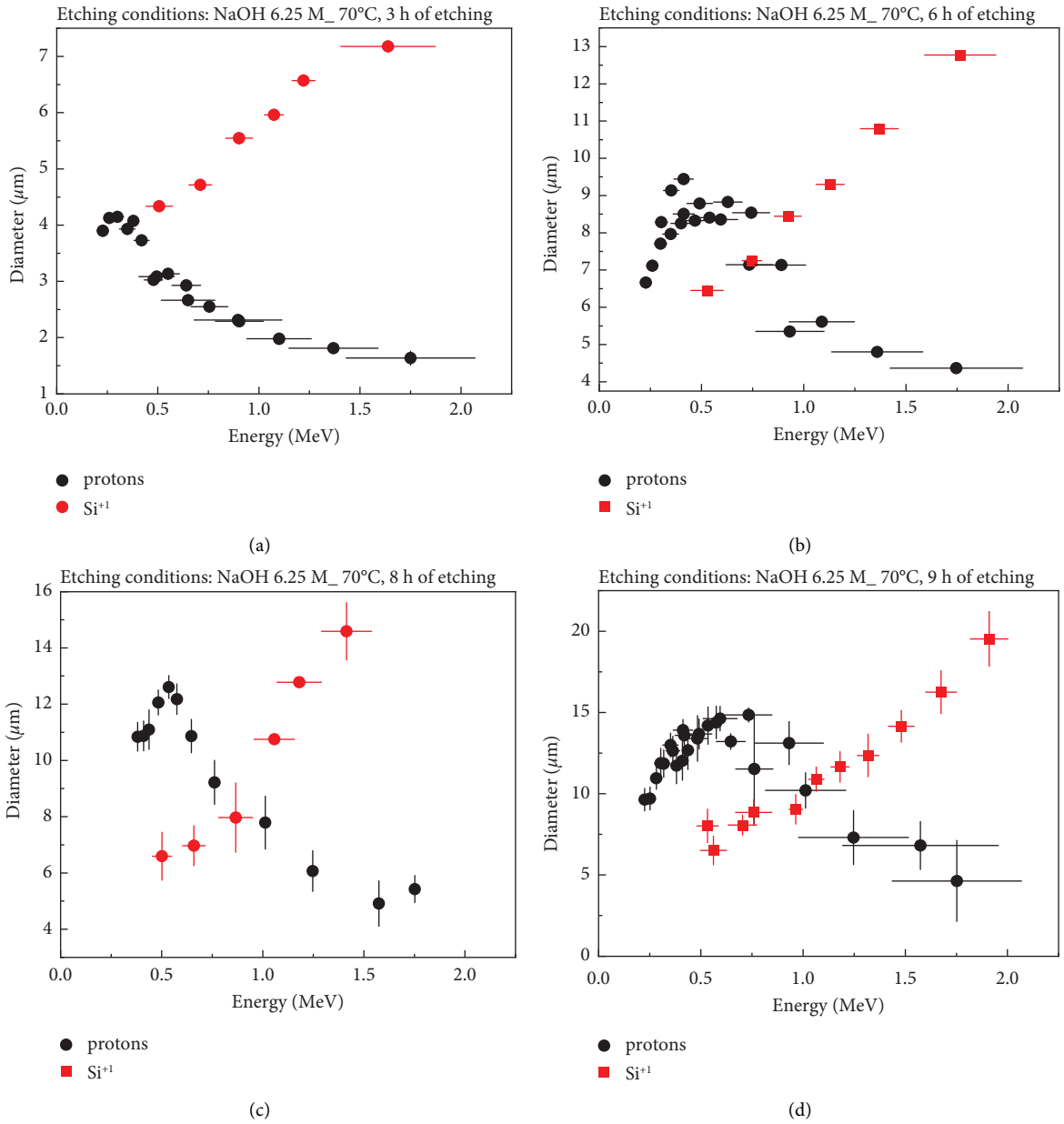

FIGURE 8: Diameter versus energy of protons and Si^{+1} ions at different etching times: 3 h (a), 6 h (b), 8 h (c), and 9 h (d), revealing that the particles are fully discriminated only in the first 3 h of etching.

The proposed methodology relies on the fact that the tracks of protons and alpha particles start to appear at different etching times due to their difference in size and energy. The tracks of the same ion with different energy also appear at different etching times. The tracks that correspond to higher energies form smaller and deeper tracks that appear later on during the etching procedure. Therefore, we propose that the minimum etching time where the alpha particles are detected without the appearance of the proton tracks should be determined experimentally. With our microscope and the current experimental conditions, we clarified that the proton tracks are visible but not well defined in the first hour of etching. In Figure 11 we can see the tracks of 500 keV protons after 1 h of etching, revealing that the proton tracks are barely noticeable and below the resolution of our microscope. This is the reason why we present the calibration curve of protons for etching times above 2 h.

At 1 h of etching, the diameter of the alpha tracks varies between 1.5–2.8 μm, for energies between 0.6 and 3.7 MeV, which is just above the resolution of our microscope (protons have diameters below 1 μm). Concluding that after 1 h of etching and by the use of the specific magnification, we are able to detect tracks that correspond to alpha particles with energies between 0.6 and 3.7 MeV without the interference of the proton tracks. However, this does not mean that we cannot measure alpha particles with higher energies using this calibration curve. The use of appropriate filters in front of the CR-39 detectors during an experiment results to

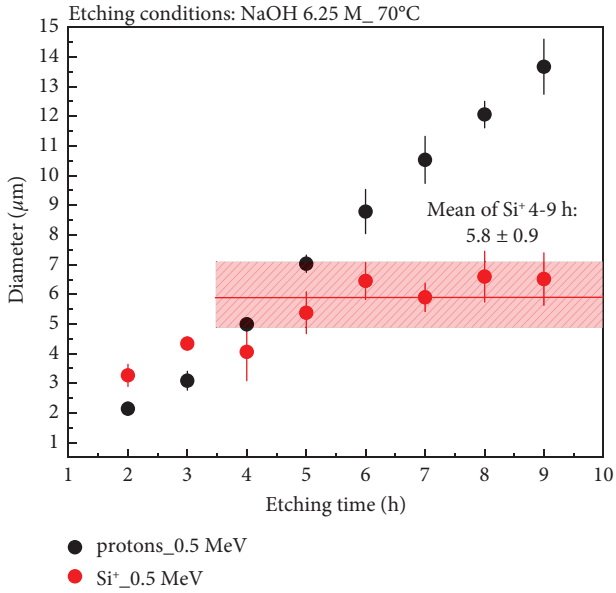

FIGURE 9: The track size of Si^+ and protons of 0.5 MeV through all etching times reveals the difference in their etching growth.

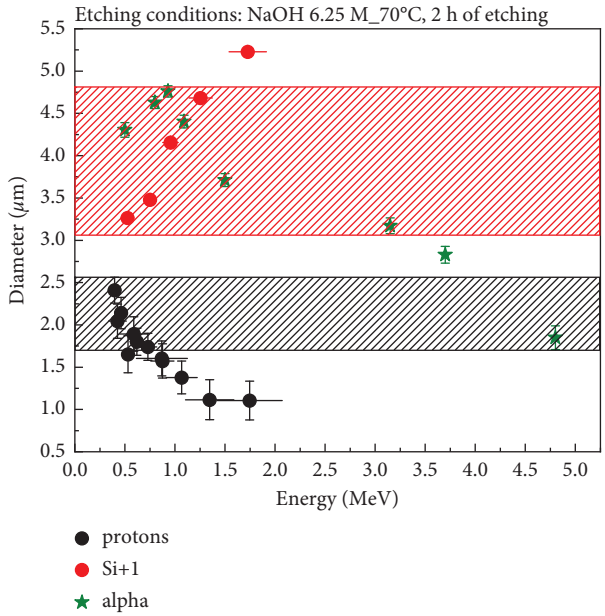

FIGURE 10: Diameters versus energy for protons and silicon ions as they were produced from TP and alpha particles calculated from a specified experiment in AN2000 and CN accelerators in LNL-INFN in Legnaro, Italy. The graph reveals an overlapping in the diameters of alpha tracks with the silicon tracks (red area) that correspond to energies below 1.5 MeV and in a smaller scale with the proton tracks of an energy below 0.8 MeV (black area).

the measurement of the remaining energy of the ion tracks. The measured energy corresponds to an initial energy (before the filter) by the addition of the energy loss inside the filter, which can be easily calculated by SRIM or LISE software [44, 45]. In this way, the calibration curve can be extended to the detection of higher energies.

Additionally, filters of different thicknesses of materials could be used in front of the CR-39 detector or the IP inside the TP spectrometer during the calibration procedure. Within this methodology (differential filtering), the different filters are placed along the parabolas in order to exclude O, C, and other heavier ions [46, 47].

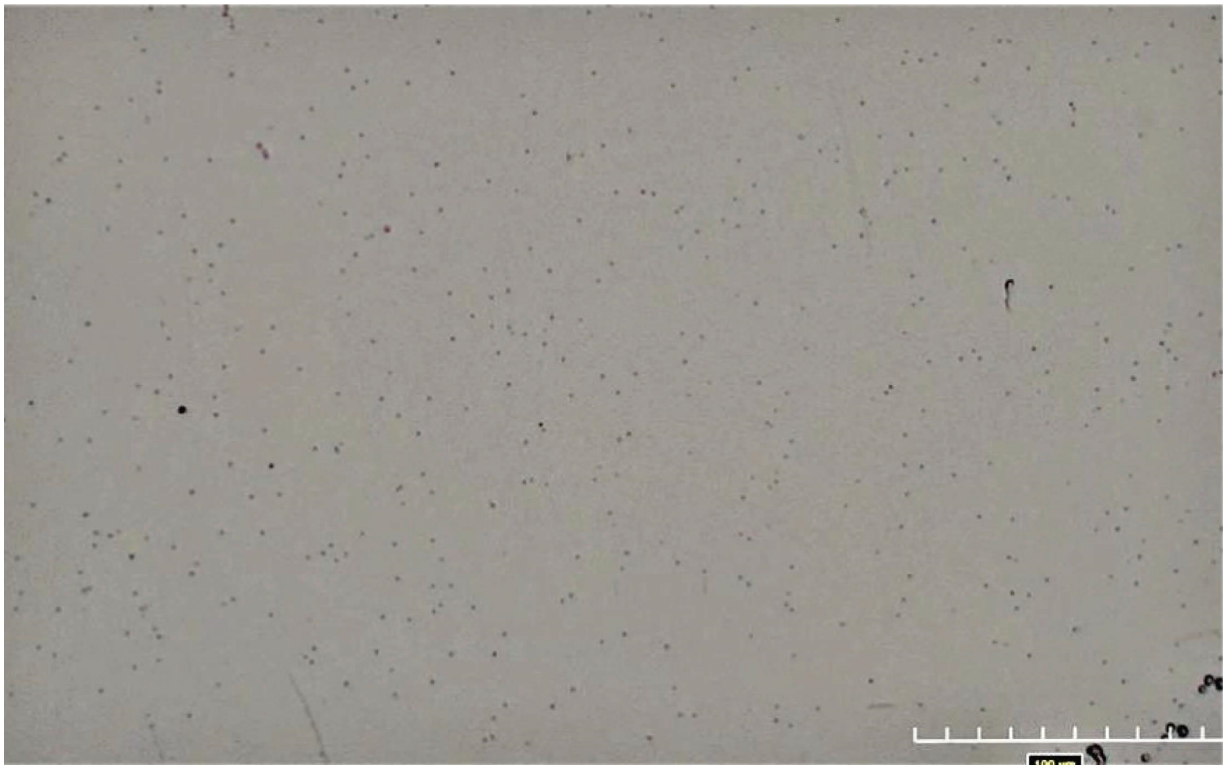

Figure 11: Tracks of 500 keV protons after 1 h of etching. The tracks start to appear but is not possible to analyze them by our microscope at the specific magnification.

4. Conclusions

Within this study, a methodology is established for the discrimination of alpha particles from other ions in the framework of a $p^{11}B$ nuclear fusion experimental campaign. For this reason, a calibration of CR-39 nuclear track detectors for protons and silicon ions was achieved through the use of a TP spectrometer. The results for the proton tracks that correspond to energies between 0.22 and 1.75 MeV were verified from previous studies. The calibration of Si ions is rarely reported in literature and never (to our knowledge) presented so extensively as in this work. The dimension of the tracks that belong to Si ions with energies between 0.56 and 12.9 MeV was achieved. The difference of the etching growth of the tracks of different ions is documented and used for the discrimination of the detected particles. The comparison of the calibration curves of alpha particles, protons, and silicon ions showed that the detectors should be used with caution because of the possible overlapping of the dimension of the tracks from different plasma ions (or energies from the same species) and alpha particles from $p^{11}B$ fusion. Furthermore, the results confirmed that CR-39 detectors can distinguish different ions at low etching times. This procedure can be extended to any other ion species (e.g., C, N, etc.) that is present in the target hosting the HB fuel in $p^{11}B$ fusion related experiments and at higher energies by the use of filters in front of the CR-39 detectors. Although the present experimental procedure was proved inefficient for the calibration of tracks of alpha particles, the experiment will be repeated using foils in front of the CR-39 detectors, this time to filter the ions carrying a higher charge and avoid the saturation effect so that the detection of alpha particles would also be possible.

Data Availability

The data used to support the findings of this study are available from the corresponding author upon request.

Conflicts of Interest

The authors declare that there are no conflicts of interest.

Acknowledgments

The authors want to acknowledge the Fusion Project (Fusion Studies of Proton Boron Neutronless Reaction in Laser-Generated Plasma) (2023–2025) funded by the CSNV (Commissione Scientifica Nazionale V) of the INFN (Istituto Nazionale di Fisica Nucleare).The authors thank the PALS facility staff for their technical support. This work was supported by the Ministry of Education, Youth, and Sports of the Czech Republic (Project no. LQ1606) and by the project "Advanced Research Using High Intensity Laser Produced Photons and Particles" (CZ.02.1.01/0.0/0.0/16_019/0000789). This scientific paper has been published as

part of the international project co-financed by the Polish Ministry of Science and Higher Education within the programme called "PMW" for 2023. This work has been carried out within the framework of the EUROfusion Consortium, which was funded by the European Union via the Euratom Research and Training Programme (Grant Agreement No 101052200 — EUROfusion). Views and opinions expressed are however those of the author(s) only and do not necessarily reflect those of the European Union or the European Commission. Neither the European Union nor the European Commission can be held responsible for them. The authors also acknowledge the IMPULSE Project (Integrated Management and Reliable Operations for User-based Laser Scientific Excellence), Grant Agreement number: 871161, 2020–2024.

References

[1] A. W. Morris, R. J. Akers, M. Cox et al., "Towards a fusion power plant interration of physics and technology," *Plasma Physics and Controlled Fusion*, vol. 64, Article ID 64002, 2022.

[2] M. L. E. Oliphant and E. Rutherford, "Experiments on the transmutation of elements by protons," *Proceedings of the Royal Society of London - Series A: Containing Papers of a Mathematical and Physical Character*, vol. 141, no. 843, pp. 259–281, 1933.

[3] H. Hora, G. H. Miley, M. Ghoranneviss, B. Malekynia, N. Azizi, and X. T. He, "Fusion energy without radioactivity: laser ignition of solid hydrogen-boron (11) fuel," *Energy & Environmental Science*, vol. 3, no. 4, pp. 479–486, 2010.

[4] W. Biter, S. Hess, and S. Oh, "Development status of electrostatic switched radiator," *Space Technology And Applications*, vol. 813, Article ID 2169180, 2006.

[5] L. Giuffrida, D. Margarone, G. A. P. Cirrone, A. Picciotto, G. Cuttone, and G. Korn, "Prompt gamma ray diagnostics and enhanced hadron-therapy using neutron-free nuclear reactions," *AIP Advances*, vol. 6, no. 10, Article ID 105204, 2016.

[6] G. A. P. Manti, "First experimental proof of Proton Boron Capture Therapy (PBCT) to enhance protontherapy effectiveness," *Scientific Reports*, vol. 8, no. 1, pp. 1–15, 2018.

[7] S. M. Qaim, I. Spahn, B. Scholten, and B. Neumaier, "Uses of alpha particles, especially in nuclear reaction studies and medical radionuclide production," *Radiochimica Acta*, vol. 104, no. 9, pp. 601–624, 2016.

[8] S. Stave, M. W. Ahmed, R. H. France et al., "Understanding the B11(p,α)$\alpha\alpha$ reaction at the 0.675 MeV resonance," *Physics Letters B*, vol. 696, no. 1–2, pp. 26–29, 2011.

[9] W. M. Nevins and R. Swain, "The thermonuclear fusion rate coefficient for p-11B reactions," *Nuclear Fusion*, vol. 40, no. 4, pp. 865–872, 2000.

[10] V. S. Belyaev, A. P. Matafonov, V. I. Vinogradov et al., "Observation of neutronless fusion reactions in picosecond laser plasmas," *Physical Review E - Statistical, Nonlinear and Soft Matter Physics*, vol. 72, no. 2, pp. 9–13, 2005.

[11] C. Labaune, C. Baccou, S. Depierreux et al., "Fusion reactions initiated by laser-accelerated particle beams in a laser-produced plasma," *Nature Communications*, vol. 4, pp. 1–6, 2013.

[12] A. Picciotto, D. Margarone, A. Velyhan et al., "Boron-proton nuclear-fusion enhancement induced in boron-doped silicon targets by low-contrast pulsed laser," *Physics Reviews X*, vol. 4, no. 3, pp. 1–8, 2014.

[13] J. Bonvalet, P. Nicolaï, D. Raffestin et al., "Energetic α -particle sources produced through proton-boron reactions by high-energy high-intensity laser beams," *Physical Review E - Statistical Physics, Plasmas, Fluids, and Related Interdisciplinary Topics*, vol. 103, no. 5, pp. 1–11, 2021.

[14] D. Margarone, J. Bonvalet, L. Giuffrida et al., "In-target proton–boron nuclear fusion using a PW-class laser," *Applied Sciences*, vol. 12, no. 3, pp. 1–7, 2022.

[15] L. Giuffrida, F. Belloni, D. Margarone et al., "High-current stream of energetic α particles from laser-driven proton-boron fusion," *Physical Review E - Statistical Physics, Plasmas, Fluids, and Related Interdisciplinary Topics*, vol. 101, no. 1, pp. 1–13, 2020.

[16] F. Belloni, "On a fusion chain reaction via suprathermal ions in high-density H–11B plasma," *Plasma Physics and Controlled Fusion*, vol. 63, no. 5, 2021.

[17] F. Consoli, R. De Angelis, and P. Andreoli, "Diagnostic methodologies of laser-initiated 11B(p,α)2α fusion reactions," *Frontiers in Physiology*, vol. 8, 2020.

[18] F. Bahrami, F. Mianji, R. Faghihi, M. Taheri, and A. Ansarinejad, "Response of CR-39 to 0.9-2.5 MeV protons for KOH and NaOH etching solutions," *Nuclear Instruments and Methods in Physics Research, Section A: Accelerators, Spectrometers, Detectors and Associated Equipment*, vol. 813, pp. 96–101, 2016.

[19] K. Jungwirth, "The Prague Asterix laser system," *Physics of Plasmas*, vol. 8, no. 5, pp. 2495–2501, 2001.

[20] K. Harres, "Development and calibration of a Thomson parabola with microchannel plate for the detection of laser-accelerated MeV ions," *Review of Scientific Instruments*, vol. 79, no. 9, pp. 1–9, 2008.

[21] S. Chaurasia, V. Rastogi, and D. S. Munda, "Thomson parabola: a high resolution ion spectrometer," *BARC Newslatter*, vol. 2, 2015.

[22] SIMION, "The field and particle trajectory simulator Industry standard charged particle optics software," 2020, https://simion.com/.

[23] S. L. Guo, B. L. Chen, and S. A. Durrani, "Solid-state nuclear track detectors," *Journal of Materials Science*, vol. 275, no. 96, 2012.

[24] T. W. Jeong, "CR-39 track detector for multi-MeV ion spectroscopy," *Scientific Reports*, vol. 7, no. 1, pp. 2–9, 2017.

[25] A. Malinowska, M. Jaskóła, A. Korman, A. Szydłowski, and M. Kuk, "Characterization of solid state nuclear track detectors of the polyallyl-diglycol-carbonate (CR-39/PM-355) type for light charged particle spectroscopy," *Review of Scientific Instruments*, vol. 85, no. 12, Article ID 123505, 2014.

[26] K. Malinowski, E. Skladnik-Sadowska, and M. J. Sadowski, "Comparison of responses of LR-115A, CR-39 and PM-355 track detectors to pulsed low-energy proton streams," *Radiation Measurements*, vol. 40, no. 2–6, pp. 371–374, 2005.

[27] H. A. Khan, R. Brandt, N. A. Khan, and K. Jamil, "Track-registration-and-development characteristics of CR-39 plastic track detector," *Nuclear Tracks and Radiation Measurements*, vol. 7, no. 3, pp. 129–139, 1983.

[28] M. Seimetz, "Spectral characterization of laser-accelerated protons with CR-39 nuclear track detector," *Review of Scientific Instruments*, vol. 89, no. 2, 2018.

[29] J. Rojas-Herrera, "Impact of x-ray dose on the response of CR-39 to 1-5.5 MeV alphas," *Review of Scientific Instruments*, vol. 86, no. 3, 2015.

[30] C. Baccou, "CR-39 track detector calibration for H, He, and C ions from 0.1-0.5 MeV up to 5 MeV for laser-induced nuclear

fusion product identification," *Review of Scientific Instruments*, vol. 86, no. 8, pp. 0–9, 2015.

[31] X. J. Duan, "Calibration of solid state nuclear track detector CR-39 with monoenergetic protons," *Wuli Xuebao/Acta Physica Sinica*, vol. 59, no. 5, pp. 3147–3153, 2010.

[32] Y. Zhang, "Energy calibration of a CR-39 nuclear-track detector irradiated by charged particles," *Nuclear Science and Techniques*, vol. 30, no. 6, pp. 1–9, 2019.

[33] R. K. Jain, A. Kumar, and B. K. Singh, "Track etch parameters and annealing kinetics assessment of protons of low energy in CR-39 detector," *Nuclear Instruments and Methods in Physics Research Section B: Beam Interactions with Materials and Atoms*, vol. 274, pp. 100–104, 2012.

[34] G. Immè, D. Morelli, M. Aranzulla, R. Catalano, and G. Mangano, "Nuclear track detector characterization for alpha-particle spectroscopy," *Radiation Measurements*, vol. 50, pp. 253–257, 2013.

[35] N. Sinenian, "The response of CR-39 nuclear track detector to 1–9 MeV protons," *Review of Scientific Instruments*, vol. 82, no. 10, 2011.

[36] B. Dörschel, D. Fülle, H. Hartmann, D. Hermsdorf, K. Kadner, and C. Radlach, "Dependence of the etch rate ratio on the energy loss in proton irradiated CR-39 detectors and recalculation of etch pit parameters," *Radiation Protection Dosimetry*, vol. 71, no. 2, pp. 99–106, 1997.

[37] E. Skladnik-Sadowska, J. Baranowski, and M. Sadowski, "Low-energy ion measurements by means of CR-39 nuclear track detectors," *Radiation Measurements*, vol. 34, no. 1–6, pp. 337–339, 2001.

[38] A. Picciotto, D. Margarone, J. Krasa et al., "Laser-driven acceleration of protons from hydrogenated annealed silicon targets," *Europhysics Letters Association Europhysics Letters*, vol. 92, no. 3, 2010.

[39] A. Picciotto, D. Margarone, M. Crivellari et al., "Microfabrication of silicon hydrogenated thin targets for multi-MeV laser-driven proton acceleration," *Applied Physics Express*, vol. 4, no. 12, pp. 2–5, 2011.

[40] A. Picciotto, M. Crivellari, P. Bellutti et al., "Fabrication of advanced targets for laser driven nuclear fusion reactions through standard microelectronics technology approaches," *Journal of Instrumentation*, vol. 12, 2017.

[41] HIROX, "High-Range Triple Zoom Lens," 2022, https://hirox-europe.com/products/3d-digital-microscope/lenses/mxb-2500rez-mxb-5000rez/.

[42] ImageJ, "Image Processing and Analysis in Java," 2022, https://imagej.nih.gov/ij/.

[43] Accelerator Division, "Accelerator Division," 2022, https://www1.lnl.infn.it/%7Esda/.

[44] J. P. Biersack, J. F. Ziegler, and M. D. Ziegler, "Srim - the stopping and range of ions in matter," *Nuclear-instruments-and-methods-in-physics-research-section-b-beam-interactions-with-materials-and-atoms*, vol. 268, no. 11-12, pp. 1818–1823, 2010.

[45] M. P. Kuchera, O. B. Tarasov, D. Bazin, B. Sherril, and K. V. Tarasova, "LISE++ software updates and future plans," *Journal of Physics: Conference Series*, vol. 664, no. 7, 2015.

[46] D. O. Golovin, S. R. Mirfayzi, S. Shokita et al., "Calibration of imaging plates sensitivity to high energy photons and ions for laser-plasma interaction sources," *Journal of Instrumentation*, vol. 16, no. 2, 2021.

[47] A. Alejo, S. Kar, H. Ahmed et al., "Characterisation of deuterium spectra from laser driven multi-species sources by employing differentially filtered image plate detectors in Thomson spectrometers," *Review of Scientific Instruments*, vol. 85, no. 9, pp. 1–7, 2014.